Submitted to *Thin Solid Films*

(to appear in 2007)

Physical properties of erbium implanted tungsten oxide films deposited by reactive dual magnetron sputtering

Sodky H. Mohamed[1,2] and André Anders[1]

[1]Lawrence Berkeley National Laboratory, 1 Cyclotron Road, California 94720, USA

[2]Physics Department, Faculty of Science, Sohag University, 82524 Sohag, Egypt

Abstract

Amorphous and partially crystalline WO_3 thin films were prepared by reactive dual magnetron sputtering and successively implanted by erbium ions with a fluence in the range from 7.7×10^{14} to 5×10^{15} ions/cm^2. The electrical and optical properties were studied as a function of the film deposition parameters and the ion fluence. Ion implantation caused a strong decrease of the resistivity, a moderate decrease of the index of refraction and a moderate increase of the extinction coefficient in the visible and near infrared, while the optical band gap remained almost unchanged. These effects could be largely ascribed to ion-induced oxygen deficiency. When annealed in air, the already low resistivities of the implanted samples decreased further up to 70ºC, whereas oxidation, and hence a strong increase of the resistivity, was observed at higher annealing temperatures.

Keywords: Dual magnetron sputtering; tungsten oxide films; Er ion implantation, electrical resistivity, optical properties

Introduction

Transition metal oxides doped with rare earth ions have received much attention because they are very useful for optical devises applications [1], electrolytes for solid oxide fuel cells [2], optical waveguides [3], and for counter electrodes in electrochromic devices [4]. Particularly, erbium (Er) ion implanted and/or doped transition metal oxides are promising for optoelectronic applications. Er-doped fiber amplification is based on the optical properties of this ion [1], and Er-ion-doped TiO_2 and ZrO_2 are being used as planar optical waveguides [3,5].

Tungsten oxide (WO_3) thin films have been thoroughly examined because of their remarkable optical, electrical and electrochromic properties [6-8], which are used in smart windows, optical displays, and reflectance-modulating automobile rear-view mirrors [6]. WO_3 is also used as an active layer in gas sensors since it has the ability to decrease its high resistance when certain gasses are adsorbed [7,8]. Rare earth (Am, Cm, Nd and Eu) doped tungsten oxide bronzes were synthesized as inert matrices used in the study of transmutation of long-life actinide isotopes [9]. Rare earth (Nd, Yb and Y) doped tungsten oxynitrides with a defect fluorite-type structure were synthesized as pigments [10].

In this contribution, we study the effects of Er ion implantation on WO_3 thin films that were synthesized by dual reactive magnetron deposition at various deposition temperatures. In particular, we focus on the electrical resistivity and optical properties at room temperature and after annealing in air.

2. Experimental details

WO_3 films were prepared on microscope glass slides (borosilicate with chemical composition of 96.4 % SiO_2, 3.0 % B_2O_3, 0.5 % Al_2O_3 and 0.1 % miscellaneous traces) and

on Si (100) substrates using reactive dual magnetron sputtering of metallic tungsten targets in an argon and oxygen gas mixture. Oxygen was feed into the processing system through a plasma source of the Constricted Plasma Source type [11] operated at 1500 W. The plasma source was positioned between two magnetrons. Its purpose of the plasma source was to enhance the activation of the reactive gas by providing a higher density of ions, excited atoms, and molecules. For this work, no further studies were done to quantify the effects of the plasma source, as opposed to using the reactive gas only. Argon was supplied to the sputtering region via a separate gas inlet. The flow of the gases (O_2, Ar) was controlled by mass flow controllers. The magnetrons (Angstrom Sciences) had rectangular tungsten cathodes, 17.5 cm x 5 cm.

Sputtering was started with the substrates either at room temperature, or preheated at 50ºC or 200ºC. The substrate was constantly moved, back and forth, in front of the two magnetrons and the plasma source; the closest distance between substrate and these targets was 5 cm. A contactless, infrared temperature sensor (RayTek®) was moving with the substrate, recording the temperature of the substrate's backside surface. The final temperature after sputtering was determined to be 155ºC, 178ºC and 202ºC for the samples started at room temperature, preheated to 50ºC, and 200ºC, respectively. The cryogenically pumped vacuum system had a background pressure better than 1.3×10^{-4} Pa at full pumping speed (1500 /s for air) and about 1.3×10^{-3} Pa at the reduced speed used during sputter deposition. The throttling by an adjustable valve (VAT Inc) was necessary to use relatively high pressure and cryogenic pump. The total pressure during deposition was kept constant at 5.3 Pa (40 mTorr) monitored by a Baratron® capacitance manometer. The oxygen to argon partial pressures ratio was 0.31 as determined by a differentially pumped gas monitor (PPM 100 by SRS). This gas monitor was pre-calibrated via the readings of the Baratron.

The sputtering power was provided by a SPIK2000A pulser (Melec GmbH) fed by a Pinnacle dual power supply (Advanced Energy). The frequency was set to 50 kHz and the power of 1.5 kW was equally shared between the two magnetrons.

After sputtering, the films were taken from the deposition chamber and mounted on a holder for installation in the metal ion implanter. We used a broad beam vacuum arc ion source of the "Mevva V" type [12] that can deliver high current pulsed metal ion beams. The beam contains several ion charge states as produced in the vacuum arc. For erbium, the charge state distribution is approximately 1%, 63%, 35%, and 1% for the ion charge states $Q = 1$, 2, 3 and 4, respectively. The ion extraction voltage was set to 50 kV, leading to a mixture of ion energies in the beam given by $E_i\left(Q\right) = QeV_{extract}$, i.e., 1% of ions had energy 50 keV, 63% had 100 keV, 35% had 150 keV, and 1% had 200 keV. The charge-state-averaged ion energy was 118 keV. The fluence of the beam was determined by a calibrated Faraday cup (the secondary electrons were magnetically suppressed). After ion beam calibration, the WO_3 films were ion implanted with various fluences in the range from 7.7×10^{14} to 5×10^{15} erbium ions/cm^2.

Glass slide substrates were used for x-ray diffraction (XRD) because of their amorphous structure, and for measurements of the optical properties because of the high transparency in the visible range. Si(100) substrates were used for film thickness measurements (Dektak IIA profilometer). The Film thickness was in typically in the range of 300 nm as revealed by the profilometer and by optical measurements by using interference fringes.

The crystallographic structure of the films was determined by XRD using a Siemens D-500 diffractometer with a Cu tube operated at 40 kV and 30 mA. The measurements

were carried out using Cu K_α radiation with a Ni filter to remove the Cu K_β reflections.

The spectral transmittance, *T*, and reflectance, *R,* were measured near normal incidence (8° off-normal) using a Perkin-Elmer Lambda-19 spectrophotometer in the wavelength range λ=300-2500 nm.

The glass slides had pre-sputtered silver contacts of well-defined length and distance, allowing us to record the sheet resistance of the films using a two-terminal configuration. The electrical contacts pads were made by masked silver sputtering, similar to previous work [13]. After film deposition, the room temperature-resistance was determined using a digital multimeter (Fluke model 189). For a study of the temperature dependence of the resistivity, some of the samples were placed in an oven for annealing in air without illumination at different temperatures and for different times.

3. Results and Discussions

3.1 Film composition and structure

The Er concentration profiles in WO_3 films were simulated using the dynamic TRIM (transport of ions in matter [14]) code “T-DYN 4.0” [15]. Figs.1a-e show the Er depth profiles for different fluences. Because sputtered films are known to have a density less than bulk density, and the values of our films are not known, the simulation was done for various densities. The high end of the density is given by the WO_3 bulk value of 7.2 g/cm^3. On the low density side we used 4.5 g/cm^3, as Jin *et al.* [16] determined for direct current-sputtered WO_3 films.

The Figs. 1 a-e show that the maximum Er concentration that can be reached is 2.5 at.% at the highest fluence of 5×10^{15} ions/cm^2. As expected, denser films have a greater stopping power and therefore the depth of penetration (or more precisely, the projected range) depends on the film density. Most ions come to rest at a depth of about 50 nm, which is smaller than the

film thickness.

XRD patterns revealed that all the samples prepared without pre-heating and the samples prepared at 50ºC were amorphous before and after implantation. The implanted samples did not show any diffraction peaks that could be associated with erbium. The films prepared with pre-heating at 200ºC were partially amorphous and partially crystalline (Fig. 2a), and they showed a characteristic crystalline peak at 23.37º which corresponds to (020) of the triclinic WO_3 [17]. After Er ion implantation, the (020) peak diminished, indicating amorphization of the material (Fig. 2b), a well-known effect of ion implantation at low temperature.

3.2 Electrical Properties

The room-temperature resistivities of WO_3 films (before implantation) were 4.92×10^7, 4.21×10^7 and 4.77×10^7 Ωcm for the films deposited without preheating, with preheating at 50ºC, and preheating at 200ºC, respectively. These values are higher than the typical reported values of 10^3-10^7 Ωcm for radio-frequency-sputtered WO_3 films [18]. It is known from the literature that the conductivity of WO_3 films depends on the stoichiometry of the films, which is greatly affected by the O_2/Ar ratio during sputtering [18]. According to Gillet *et al.* [19], the conductivity of WO_3 is enhanced and determined by the presence of oxygen vacancies. For example, the suboxide $W_{18}O_{49}$ exhibited very low electrical resistivity of 1.75×10^{-3} Ωcm [20]. The high resistivity of our as-deposited films can be ascribed to the presence of activated oxygen in the deposition process, supplied by the constricted plasma source, which lead to insulating, stoichiometric WO_3.

Figure 3 shows that Er ion implantation dramatically reduces the resistivity of the originally highly insulating films. The decrease in resistivity by several orders of magnitude can be ascribed to two major effects that lead to carrier generation. The first effect is the loss of

oxygen and the formation of substoichiometric oxides (WO_{3-x}). Following [21], the process can be described as follows:

$$O^{2-} \text{ (lattice)} \rightarrow 1/2\ O^2 \text{ (interstitial or leaving the film)} + 2e^- \text{ (conduction).} \qquad (1)$$

The oxygen vacancies in the substoichiometric oxides can be neutral (V^0), singly charged (V^+), or doubly charged (V^{2+}), with respect to the undisturbed lattice [22]. A neutral vacancy displays an electron concentration similar to that of the stoichiometric compound. However, it is energetically advantageous to transfer one or both of its electrons to neighboring tungsten ions.

In the case of a V^+ vacancy, the vacancy electrons tends to form a bond with one W^{6+} ion while the other neighboring tungsten ions are in the W^{5+} state. In the case where two electrons transfer to one neighboring tungsten ion, the tungsten is in the W^{4+} state, while the vacancy is doubly charged. The two electrons may also transfer to two neighboring tungsten ions forming a doubly charged vacancy and two W^{5+} ions. The two W^{5+} ions will move closer to one another forming a doubly charged $(W\text{-}W)^{10+}$ complex. The above mentioned oxidation states (ions) can lead to enhanced conductivity [23,24].

The second effect is the generation of carriers due to the ion-induced displacements and defects. Both mechanisms are effective because Er is a relatively large ion, hence the stopping power is large and the ion energy is deposited in a small damage volume below the surface.

It is further observed that for each of the investigated Er fluences, the decrease in resistivity depended on the original film preparation temperature. The films prepared with preheating at 200ºC had the lowest resistivity. It is reasonable to presume that subtle differences in the pre-implantation structure (like the presence of small crystalline grains at higher temperature) affected the concentration of carriers and their mobility.

Annealing of the implanted samples in normal air up to 70ºC lead to a decrease in resistivity. This can be ascribed to (i) ionization of shallow traps due to defect states, and (ii)

desorption of oxygen, which usually is adsorbed on the surface of the film and may act as traps for electrons.

Annealing the implanted samples at temperatures higher than 70ºC leads to increase the resistivity. Figure 4 shows the increase of the room temperature resistivity for the films implanted with an Er fluence of 5×10^{15} ions/cm^2. In this experiment, the annealing temperature was 100ºC (note that for each data point, the samples were cooled down to room temperature before the data point was taken). It can be seen that the increase in resistivity is more pronounced for the samples prepared without preheating. Annealing the implanted samples at 300°C for 10 min leads to a drastic increase in resistivity, the resistivity increases to the range 10^7 Ωcm. The increase in resistivity upon annealing at temperatures higher than 70ºC is attributed to the oxidation of some oxygen vacancies [19]. Possibly the borosilicate substrate degrades upon annealing for long time and affects the resistivity. This effect, however, should be very small since it is observed from Fig. 4 that the major increase in resistivity happened after annealing for 5 h. Xu *et al.* [23] have studied the variation of the conductivity of sputtered WO_3 films with temperature on different substrate materials. They found that the conductivity of sputtered WO_3 films is strongly temperature dependent and appears to be independent of the substrate, since the results obtained from alumina and silica substrates were similar with the YZ $LiNBO_3$.

3.3 Optical Properties

Figure 5a-c shows the spectral transmittance, *T*, of WO_3 thin films before and after Er ion implantation (fluence from 7.7×10^{14} to 5.0×10^{15} ions/cm^2). It can be observed that *T* for pristine (unimplanted) WO_3 films is very high (greater than 90%, solid lines). High transmission, the occurrence of interference oscillations, and a sharp decrease at the

absorption edge indicate good optical quality of the films. Upon Er ion implantation, the spectral transmission gradually decreased and the interference oscillations were strongly damped as the Er ion fluence was increased. This indicates that the Er-implanted samples are very defective with a broad range of energetic defect positions.

The decrease in transmittance is visible as a change from colorless to progressively grey with increasing ion fluence, which can be attributed to oxygen deficiency [25]. The grey coloration is fully reversible upon heating the samples in normal air above 70 ºC. It is further noticed that the WO_3 samples prepared at 200ºC are more affected by the Er implantation than the samples prepared without preheating.

Using the measured spectral transmittance and reflectance, and the film thickness, *d*, the absorption coefficient α was calculated according to

$$\alpha = \frac{1}{d} \ln\left(\frac{1-R}{T}\right). \qquad (2)$$

The optical band gap, E_g, was determined by [26]

$$\alpha h\nu = \beta(h\nu - E_g)^r \qquad (3)$$

where β is a constant and *r* is equal to 2 or ½ for allowed indirect or direct transitions, respectively. The E_g values were extracted from the $(\alpha h\nu)^{1/2}$ vs. $h\nu$ plot, indicating an indirect band gap for all of the pristine and implanted films. The obtained E_g values are listed in Table 1. The calculated standard deviation values are 0.033, 0.038, and 0.041 for the E_g values of films deposited without preheating, with preheating at 50ºC, and preheating at 200ºC, respectively. It is seen that there is no obvious change in the band gap by the ion implantation. This indicates that the optical transitions are happening through extended states and not through the localized states in the optical band gap. However, the implantation experiments favor the creation of localized states in the band gap. This can be explained

according to Anderson's model [27] where the localized states are doubly occupied with electrons; hence, they are self-trapped to below the Fermi energy and cannot be excited optically. Only single-electron excitations over the mobility gap can be observed.

The refractive index values, *n*, of WO_3 films were calculated from the spectral transmittance before and after Er ion implantation using the Swanepoel method [28,29]. The results are shown in Figs. 6a-c. The refractive index decreases with increasing fluence. A similar decrease in refractive index of sol–gel deposited WO_3 and implanted with Co-60 radio isotope was observed by Zayima and Baydogan [30]. This decrease in refractive index may be attributed, as Atuchin [31] modeled for He-implanted $LiNbO_3$ and $LiTaO_3$, to an increase in molar volume and a spontaneous decrease of polarization induced by the interaction of the implanted ions with the lattice.

The extinction coefficient, *k*, of WO_3 films was determined before and after Er ion implantation from the equation

$$k = \alpha\lambda / 4\pi , \tag{4}$$

where $\alpha = \alpha(\lambda)$ is the wavelength dependent absorption coefficient (Figs. 7a-c). It is observed that the *k* values increase with increasing Er ion fluence. This can be ascribed to the creation of defect centers as well as free electrons, in agreement with the above-discussed findings of the conductivity changes.

4. Summary and Conclusions

Thin films of tungsten oxide have been deposited by plasma-assisted dual magnetron sputtering and implanted by Er ions of successively higher fluences. The pristine films were highly transparent and insulating before implantation, indicating that the oxygen plasma assistance lead to stoichiometric WO_3 films. Ion implantation caused a very large decrease

in the resistivity (from >10^7 Ωcm to <10^1 Ωcm for moderate fluence of 5 x 10^{15} ions/cm^2) and a small decreases in the spectral transmittance in the visible and near infrared. In the visible, this was evident by grey coloration of the implanted samples. The increase in the extinction coefficient, *k*, was larger in the near IR compared to the visible part of the spectrum. Electrical and optical changes are largely due to oxygen deficiencies. These changes are slightly sensitive to the temperature of the deposition process: films prepared at elevated temperature (200°C) show larger changes upon ion implantation. Annealing study done in air showed that the Er implanted WO_3 films are thermally stable up to 70ºC. When annealing above 70°C, the resistivity increases strongly and the spectral transmittance increased, too, indicating oxidation, i.e., a reduction of the oxygen vacancies.

Based on the above-described properties we can conclude that sputter deposition and ion implantation can be used to fabricate amorphous or partially crystalline WO_3 films that have specific electrical and optical properties, which could be used, for example, in sensors.

Acknowledgements

The authors are grateful for support by Sakon Sansongsiri, Michael Dickinson, and Joe Wallig. One of us (S. H. M.) would like to express his sincere gratitude to the Fulbright Commission for a fellowship to carry out this research work at Lawrence Berkeley National Laboratory. This work was supported by the Assistant Secretary for Energy Efficiency and Renewable Energy, Office of Building Technology, of the U.S. Department of Energy under Contract No. DE-AC02-05CH11231.

References

[1] C. Mignotte, Appl. Surf. Sci. 226 (2004) 355.

[2] Y. Mizutani, K. Hisada, K. Ukai, H. Sumi, M. Yokoyama, Y. Nakamura, O. Yamamoto, J. Alloys Compd. 408–412 (2006) 518.

[3] A. Bahtat, M. Bouderbala, M. Bahtat, M. Bouazaoui, J. Mugnier, M. Druetta, Thin Solid Films 323 (1998) 59.

[4] W. Chen, Y. Kaneko, J. Electroanal. Chem. 559 (2003) 83.

[5] C. Urlacher, C. Marco de Lucas, E. Bernstein, B. Jacquier, J. Mugnier, Opt. Mater. 12 (1999) 19.

[6] C. G. Granqvist, *Handbook of Inorganic Electrochromic Materials*. Amsterdam: Elsevier, 1995.

[7] M. Stankova, X. Vilanova, E. Llobet, J. Calderer, C. Bittencourt, J. J. Pireaux, X. Correig, Sens. Actuators B 105 (2005) 271.

[8] J. Guérin, K. Aguir, M. Bendahan, C. Lambert-Mauriat, Sens. Actuators *B* 104 (2005) 289.

[9] A. A. Bessonov, A. M. Fedosseev, J.-C. Krupa, I. B. Shirokova, N. A. Budantseva, J. Solid State Chem. 169 (2002) 182.

[10] N. Diot, O. Larcher, R. Marchand, J. Y. Kempf, P. Macaudiere, J. Alloys Compd. 323-324 (2001) 45.

[11] A. Anders, R. A. MacGill, M. Rubin, IEEE Trans. Plasma Sci. 27 (1999) 82.

[12] I. G. Brown, Rev. Sci. Instrum., 65 (1994) 3061.

[13] E. Byon, T. H. Oates, A. Anders, Appl. Phys. Lett. 82 (2003) 1634.

[14] J. F. Ziegler, J. P. Biersack, and U. Littmark, The Stopping and Range of Ions in Solids, New York: Pergamon Press, 1985.

[15] J. P. Biersack, Nucl. Instrum. Meth. Phys. Res. B 59/60 (1991) 21.

[16] C.-J. Jin, T. Yamazaki, Y. Shirai, T. Yoshizawa, T. Kikuta, N. Nakatani, H. Takeda, Thin Solid Films 474 (2005) 255.

[17] Powder Diffraction Files, Joint Committee on Powder Diffraction Standards, JCPDS, Card 32-1395 (1999).

[18] S. C. Moulzolf, S.-A. Ding, R. J. Lad, Sens. Actuators B 77 (2001) 375.

[19] M. Gillet, C. Lemire, E. Gillet, K. Aguir, Surf. Sci. 532-535 (2003) 519.

[20] K. Viswanathan, K. Brandt, E. Salje, J. Solid State Chem. 36 (1981) 45.

[21] H. Hosono, M. Miyakawa, H. Kawazoe, K.-I. Shimizu, J. Non-Cryst. Solids 241 (1998) 190.

[22] G. A. Niklasson, L. Berggren, A.-L. Larsson, Sol. Energy Mater. Sol. Cells 84 (2004) 315.

[23] Z. Xu, J. F. Vetelino, R. Lec, D. C. Parker, J. Vac. Sci. Technol. A 8 (1990) 3634.

[24] M. Stolze, B. Camin, F. Galbert, U. Reinholz, L. K. Thomas, Thin Solid Films 409 (2002) 254.

[25] T. J. Tate, M. Garcia-Parajo, M. Green, J. Appl. Phys. 70 (1991) 3509.

[26] J. Tauc, *Amorphous and Liquid Semiconductors*, New York: Plenum Press, 1974.

[27] P. W. Anderson, Phys. Rev. Lett. 34 (1975) 953.

[28] R. Swanepoel, J. Phys. E: Sci. Instrum. 16 (1983) 1214.

[29] E. R. Shaaban, N. El-Kabnay, A. M. Abou-sehly, N. Afify, Physica B: Cond. Matter 381 (2006) 24.

[30] E. O. Zayima, N. D. Baydogan, Sol. Energy Mater. Sol. Cells 90 (2006) 402.

[31] V. V. Atuchin, Nucl. Instrum. Methods Phys. Res. B 168 (2000) 498.

Figure Captions

Fig. 1 Er concentration versus depth as calculated by dynamic TRIM Mote Carlo simulations, assuming different WO_3 film density.

Fig. 2 X-ray diffraction patterns of WO_3 films prepared with preheating at 200ºC and implanted at different fluences: (a) 0.0 and (b) 5×10^{15} ions/cm^2.

Fig. 3 Variations of room temperature resistivity as a function of implanted fluence for WO_3 films prepared at different preheating temperatures.

Fig. 4 Evolution of the resistivity of WO_3 films, implanted with Er ions with a fluence of 5×10^{15} ions/cm^2, as a function of annealing time at 100ºC.

Fig. 5 Spectral transmittance of pristine and Er ion implanted WO_3 thin films: Films prepared (a) without preheating, (b) at 50ºC, and (c) at 200ºC. The thicknesses of the pristine samples (before ion implantation) were 295, 261 and 303 nm, prepared without preheating, at 50ºC and at 200ºC, respectively.

Fig. 6 Refractive index of pristine and Er ion implanted WO_3 thin films. The data points denote the calculated n values while the lines are fit functions based on the two-term Cauchy dispersion relationship; $n(\lambda) = a + b/\lambda^2$.

Fig. 7 Extinction coefficient of pristine and Er ion implanted WO_3 thin film.

Tables

Table 1 Optical band gap of pristine and Er-implanted WO_3 films.

Table 1

Er fluence (ions/cm^2)	Band gap, E_g (eV)		
	No-pre-heating	Pre-heated at 50°C	Pre-heated at 200°C
0.0	3.23	3.17	3.19
7.70×10^{14}	3.21	3.15	3.12
1.54×10^{15}	3.15	3.24	3.22
2.54×10^{15}	3.16	3.23	3.21
5.00×10^{15}	3.19	3.20	3.16
Standard Deviation	0.033	0.038	0.041

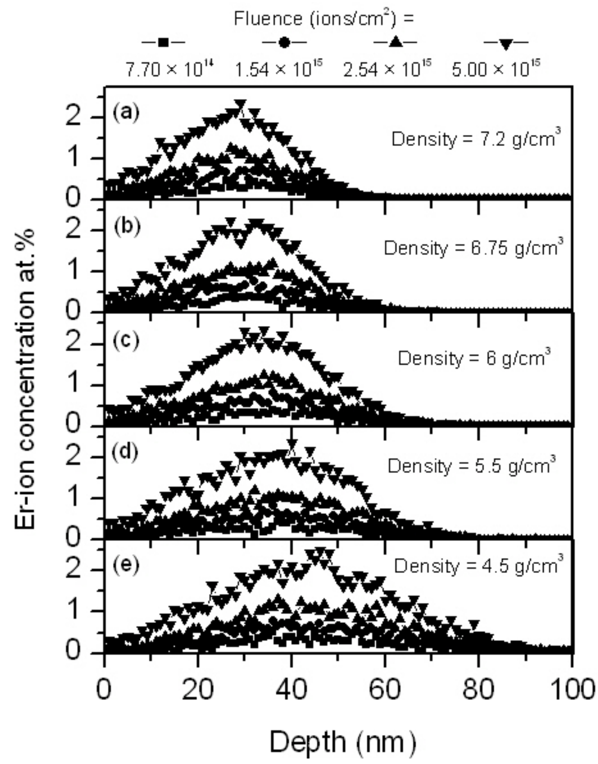

Fig. 1

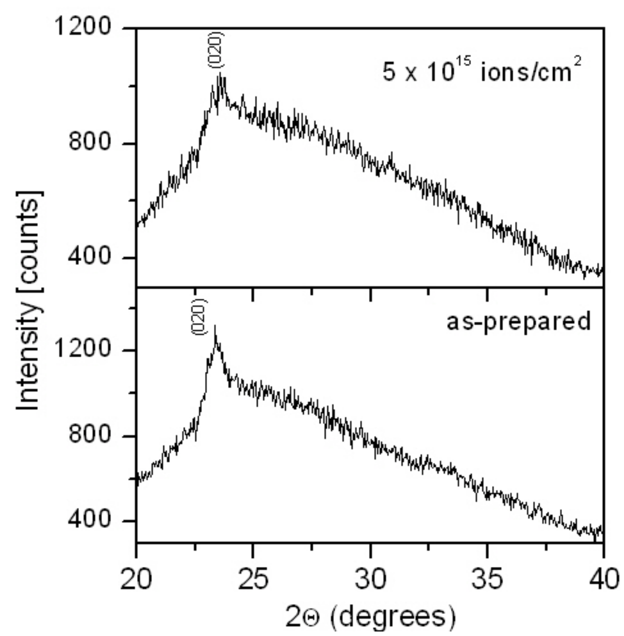

Fig. 2

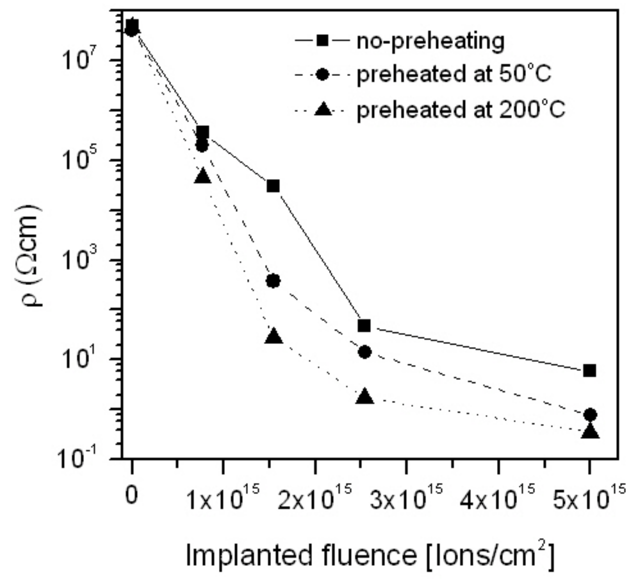

Fig. 3

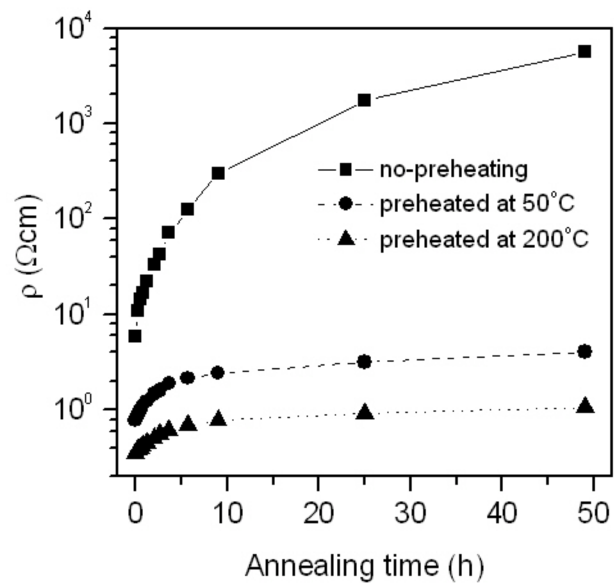

Fig. 4

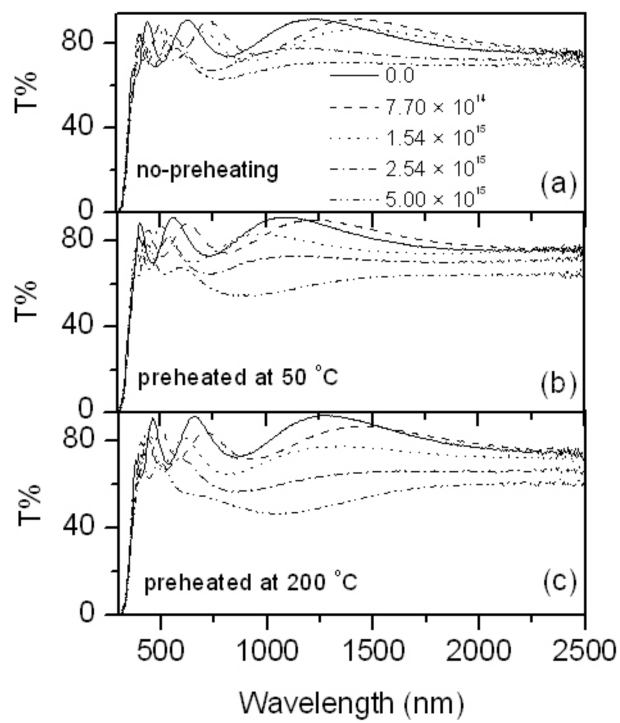

Fig. 5

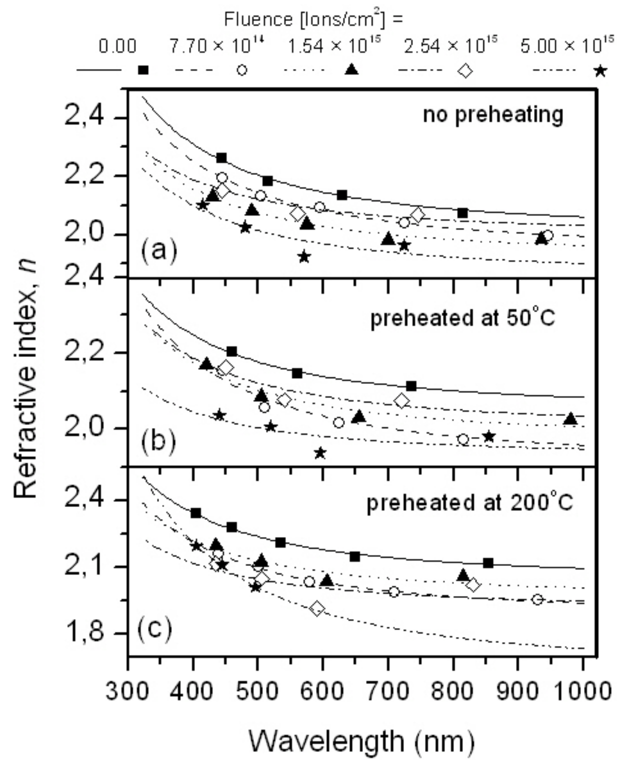

Fig. 6

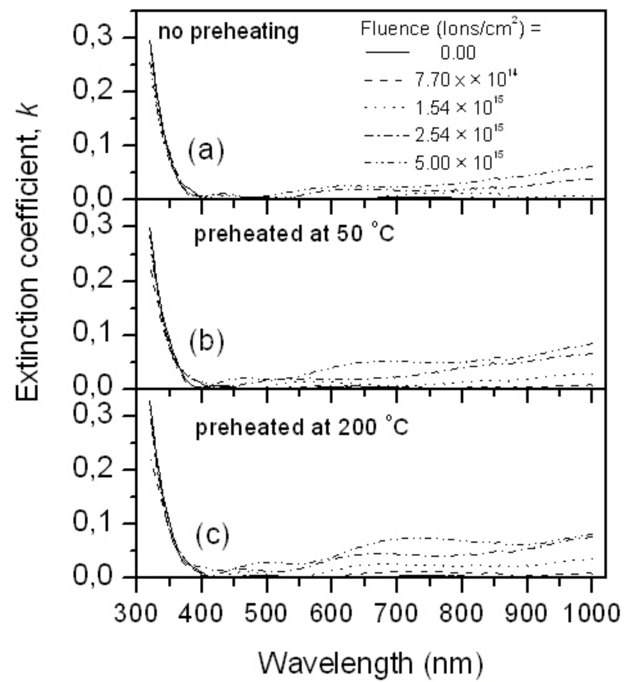

Fig. 7